OPEN ACCESS
JOURNAL OF ADVANCED DIELECTRICS
Vol. 13, No. 4 (2023) 2341001 (7 pages)

DOI: 10.1142/S2010135X23410011

Preparation and energy storage properties of ⟨001⟩-textured $NaNbO_3$-based ceramics

Zhengu Chen[*,†], Fan Chang[†], Gengguang Luo[†], Li Ma[*,†], Ju Chen[†], Jinge Pei[†], Zhenyong Cen[†], Qin Feng[†,‡,¶], Fujita Toyohisa[†] and Nengneng Luo[†,§,¶]

[*]*School of Chemistry & Chemical Engineering, Guangxi University Nanning 530004, P. R. China*

[†]*State Key Laboratory of Featured Metal Materials and Life-cycle Safety for Composite Structures School of Resources, Environment and Materials, Guangxi University, Nanning 530004, P. R. China*

[‡]fengqin307@163.com

[§]nnluo@gxu.edu.cn

Received 30 October 2022; Revised 13 January 2023; Accepted 7 February 2023; Published 10 May 2023

Dielectric materials with high energy storage density (W_{rec}) and efficiency (η) are expected for energy storage capacitors. In this work, ⟨001⟩-textured $Na_{0.7}Bi_{0.1}NbO_3$ (NBN) ceramics were prepared by a templated grain growth technique. The effects of microstructure and orientation degree on dielectric properties, polarization and energy storage performance were investigated. The textured ceramic with an optimized orientation degree (70%) showed a high W_{rec} of 2.4 J/cm^3 and η of 85.6%. The excellent energy storage properties of textured ceramic originate from the co-effect of interfacial polarization and clamping effect. The results indicate that texture development is a potential candidate to optimize the energy storage properties of functional ceramics.

Keywords: $NaNbO_3$ ceramics; grain orientation; energy storage density; dielectric capacitors.

1. Introduction

With the rapid development of electronic information technology, dielectric ceramics play a significant role in advanced electronics and electrical power due to their high power density and good cycle stability.[1–6] However, the low-energy storage density is one of the most critical factors that restricts their wide applications. In addition, environment and human health are other problems to be considered. Therefore, it is of great importance to develop environmental-friendly dielectric capacitors with high-energy storage density. Generally, the total stored energy density (W_{st}), recoverable energy density (W_{rec}) and energy storage efficiency (η) of dielectric material can be evaluated by integrating the polarization–electric field (P–E) loop based on the following mathematical formulas[4,7]:

$$W_{st} = \int_0^{P_{max}} E\mathrm{d}P, \tag{1}$$

$$W_{rec} = \int_{P_r}^{P_{max}} E\mathrm{d}P, \tag{2}$$

$$\eta = \frac{W_{rec}}{W_{st}} \times 100\%, \tag{3}$$

where E, P_{max}, P_r are the external electric field, the maximum polarization, and the remnant polarization, respectively. Hence, high E, high P_{max} and low P_r are key parameters that contribute to a high recoverable energy density.

$NaNbO_3$ (NN) ceramic is one of the promising lead-free dielectric materials for energy storage capacitors.[8] However, the pure NN ceramic exhibits low recoverable energy storage density due to the large P_r and hysteresis, as a result of the irreversible antiferroelectric (AFE)–ferroelectric (FE) phase transition at large external electric field. Therefore, various methods have been adopted to solve the problems. Stabilization of the AFE phase is an effective way to make the AFE–FE phase transition more reversible and improve the energy storage density, which can reduce the remanent polarization and improve the energy storage density to a certain degree.[9–11] Introduction of relaxor end member into NN to break the long-range AFE order into nanodomains is another way generally used, which can significantly reduce the hysteresis of P–E loops and improve the energy storage density and efficiency. Based on this logic, ultrahigh-energy storage densities were successfully achieved in $NaNbO_3$–$(Na_{0.5}Bi_{0.5})TiO_3$ relaxor AFEs.[12] Construction of an AFE–paraelectric phase boundary with high P_{max} by adding a paraelectric end member is also an effective way of improving energy storage density.[7] Besides the above-mentioned composition modification, some special preparation techniques are also adopted to tailor energy storage properties. These include optimizing

¶Corresponding authors.

sintering atmosphere,[13] employing special sintering techniques (such as spark plasma sintering,[14] liquid phase sintering,[15] cold sintering technique,[16] and two-step sintering[17]). The objectives of them are to reduce the sintering temperature, obtain dense bulk ceramics, and decrease the grain size.

Besides the above-mentioned methods, crystallographic orientation engineering also plays an important role in electrical properties.[18–21] For instance, the ⟨001⟩-textured tetragonal Pb-based piezoceramics exhibited much higher piezoelectric and dielectric responses in comparison with other oriented single crystals and nontextured ceramics.[22] In addition to the piezoelectric and dielectric properties, the polarization also exhibits orientation-dependent nature in texture ceramics. Li *et al*. demonstrated that ⟨001⟩-textured piezoelectric ceramics possessed higher P_{max}, originating from texturing enabling much more efficient alignment of the polar vectors and increasing poling efficiency.[23] On the contrary, the P_r decreases with increase of the texture fraction due to the existence of increasing interfacial stresses leading to domain motions and polarization switching becoming more difficult.[24] However, despite extensive investigations on piezoelectric properties by preparing texture ceramics, few works are focused on energy storage performance.

The template grain growth (TGG) method is a cost-effective and viable technique for producing crystallographic-oriented ceramics.[25] In the TGG process, the template particles with anisotropic shape and crystallographic properties are uniformly aligned in the matrix powders by tape cast, and the matrix powders grow epitaxially along the templated grain and resulting in textured ceramics after high-temperature sintering.[26] In particular, the structure, shape and size of template particles are critical factors to achieve high-quality textured ceramics. Besides, template particles must have a similar crystal structure and possess less than 15% lattice mismatch with the matrix particles.[27]

Based on the above consideration, the TGG was applied to the NN-based system, by using $Na_{0.7}Bi_{0.1}NbO_3$ (NBN) as a representative. The objective of this work is to prepare highly ⟨001⟩-textured NBN ceramics and study the effect of microstructure and orientation degree on polarization, dielectric properties and energy storage performance. This study may provide a new way of optimizing the high energy storage properties of dielectrics.

2. Experimental Procedure

2.1. *Synthesis of ⟨001⟩-oriented NN template*

Micron-scale platelet NN was synthesized by two-step molten salt techniques.[28] First, the platelike $Bi_{2.5}Na_{3.5}Nb_5O_{18}$ (BNN5) precursor was prepared by molten salt synthesis (MSS). The starting materials for synthesizing BNN5 are Bi_2O_3 (99.9%), Nb_2O_5 (99.99%), and Na_2CO_3 (99.9%). They were mixed according to the formula of BNN5 for 12 h in ethanol with media of zirconia balls, then NaCl as the molten salt was added into the slurry, and the mixture was subsequently milled for 12 h. After drying, the mixture was calcined in an alumina crucible at 1130°C for 3 h in air. To obtain highly purified BNN5, the product was washed with hot deionized water repetitively until the Cl^- cannot be detected by $AgNO_3$.

Then, NN was prepared by topochemical micro-crystal conversion from BNN5. First, BNN5 was mixed with Na_2CO_3 in a 1:1.5 molar ratio in ethanol and stirred gently for 12 h. Then, NaCl as the molten salt was added into the mixture and stirred for another 12 h. After drying, the mixture was heated to 960°C for 3 h in air. To remove molten salt, the products were washed several times until without Cl^-. After that, excessive nitric acid was added to the products to clear the by-products of Bi_2O_3.

2.2. *Fabrication of ⟨001⟩-textured NBN ceramics*

NBN matrix powders were synthesized by the traditional solid-state reaction method. Raw materials of Nb_2O_5 (99.99%), Na_2CO_3 (99.9%) and Bi_2O_3 (99.9%) were weighed according to stoichiometry and then ball-milled for 24 h in ethanol. After drying, the mixture was calcined at 900°C for 5 h to achieve the pure perovskite phase. The calcined powders were ball-milled again to reduce the particles to an average particle size of about 500 nm. ⟨001⟩-textured NBN ceramics were prepared by the TGG process. The tape casting slurry was prepared by dispersing NBN matrix, NN templates, dispersant (triethyl phosphate), binder (polyvinyl butyral), and plasticizer (di-n-butyl phthalate) in an ethanol–butanone solvent (60 vol.% ethanol –40 vol.% butanone). In particular, the NBN matrix and NN templates were mixed according to a molar mass ratio of 95:5. After that, ⟨001⟩-textured NBN green tapes can be obtained by tape-casting the above-prepared slurry on PET release film. After drying, the tapes were cut, stacked, and then laminated, followed by hot press and cold isostatic pressing to achieve the green ceramic body. Then they were heated to 600°C to remove organics. Finally, the samples were sintered under various conditions. For comparison, randomly oriented NBN ceramics were also prepared without adding NN templates.

2.3. *Material characterization*

The phase structure and texture quality quantified by the Lotgering factor (F_{001}) were evaluated by X-ray diffraction (XRD, D/MAX 2500V, Rigaku Co., Japan).[29] The microstructure was examined by scanning electron microscope (SEM, Phenom Pro X, Phenom-World, Eindhoven, The Netherlands). The temperature dependence of dielectric permittivity was measured by a variable temperature dielectric tester (DMS-2000, Wuhan Bailibo Co., China). The polarization versus electric field (*P–E*) hysteresis loops were measured at 10 Hz using an aixACCT TF 3000 analyzer FE measuring system (aixACCT Co., Germany). The thickness

of samples for *P–E* measurements is about 0.12 mm. The samples were printed with silver electrodes on both sides for electrical property tests.

3. Results and Discussion

The structure, shape and size of template particles are critical factors to achieve excellent textured ceramics. XRD patterns and SEM images of the BNN5 precursors are shown in Figs. 1(a) and 1(b). The diffraction peaks are well-identified by JCPDS card (No. 42-0399). The intensities of (0012), (0014) and (0024) peaks are much stronger than other peaks, indicating most of the surfaces of the BNN5 precursors are parallel to (00*l*). The BNN5 particles possess distinctly rectangular platelets with size of 10–20 μm and thickness of ~0.5 μm, which are suitable for the next step of the synthesis. Using the BNN5 as precursors, the plate-like NN particles are synthesized through ions exchange with Na_2CO_3 in the NaCl molten salt. Figure 1(c) shows the XRD pattern of the as-synthesized NN templates, which exhibit typical perovskite structure with the strongest ⟨00*l*⟩ orientation.[26] Figure 1(d) shows the SEM image of the as-synthesized NN particles, which preserve a plate-like morphology and have a relatively uniform size distributing around 10–20 μm. The preferred orientation and plate shape make them easily orient in a matrix of fine powders by the tape casting process, which helps to form a well-textured microstructure by TGG process.

Figure 2 shows the XRD patterns of the NN-templated NBN ceramics. All ceramics possess a perovskite phase without any second phase. They are mainly of orthorhombic structure according to the obvious split of the (002) diffraction peaks. The intensity of the diffraction peaks also exhibits obvious changes for the nontextured and textured ceramics. For the nontextured ceramic, the (110) diffraction peak is the strongest one, while the (001) and (002) peaks are much weaker. Interestingly, the intensity of (001) and (002) peaks continuously increases with increasing sintering temperature or time for the textured ones, accompanied by the continuous decrease in other peaks. The degree of texture can be evaluated by the Lotgering factor (F_{001}) based on the following equations[23,30,31]:

$$F_{001} = \frac{P - P_0}{1 - P_0}, \tag{4}$$

$$P = \frac{\sum I_{(00l)}}{\sum I_{(hkl)}}, \tag{5}$$

$$P_0 = \frac{\sum I_{0(00l)}}{\sum I_{0(hkl)}}, \tag{6}$$

where $\sum I_{(00l)}$ and $\sum I_{(hkl)}$ are the sum of the intensities of all (00*l*) and (*hkl*) diffraction peaks in the textured ceramics, respectively. *P* is the ratio of the two sums for the textured

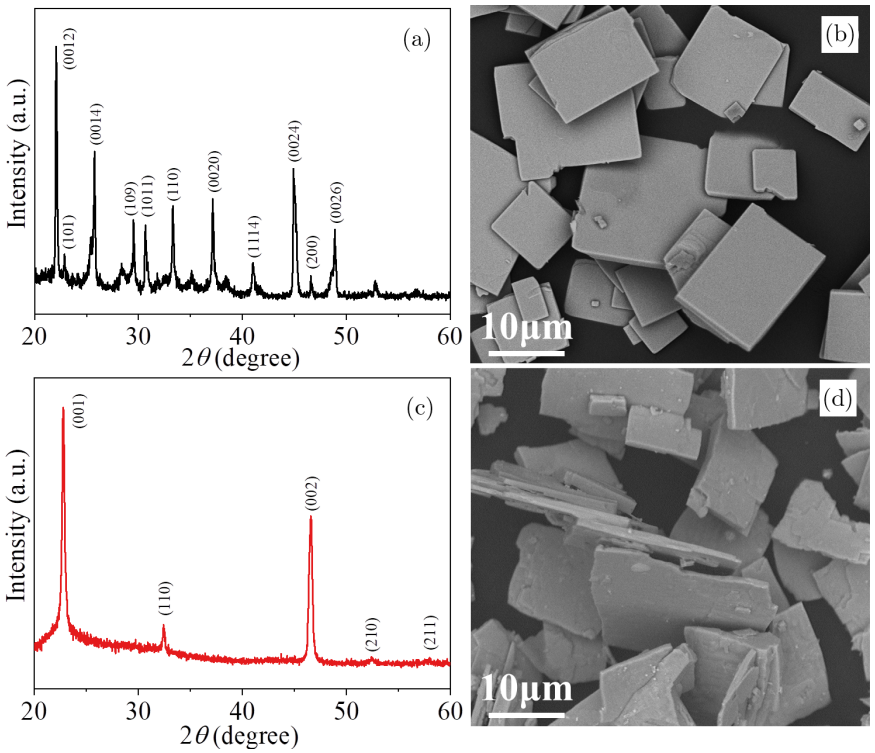

Fig. 1. (a) XRD profile and (b) SEM image of BNN5 precursors, (c) XRD profile and (d) SEM image of the NN templates.

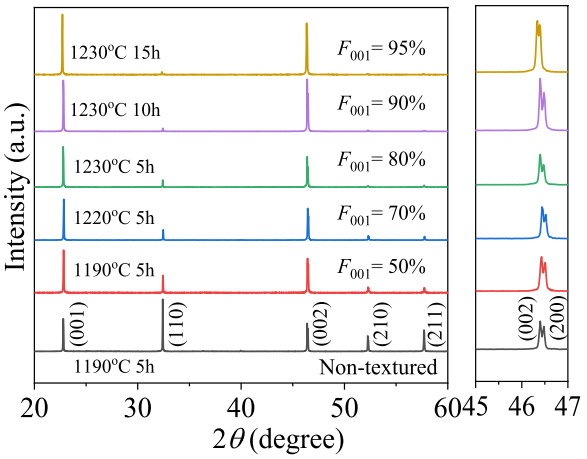

Fig. 2. XRD patterns of randomly oriented and textured NBN ceramics that sintered in different conditions.

samples. $\sum I_{0(00l)}$ and $\sum I_{0(hkl)}$ are the sum of the intensities of all (00*l*) and (*hkl*) diffraction peaks in the nontextured ceramics, respectively. P_0 is the ratio of the two sums for the nontextured sample.

Based on the equations above, a relatively low texture degree F_{001} of 50% is acquired for the textured ceramics sintered at 1190°C for 5 h due to the slow texture development. When the sintering temperature enhances to 1220°C, the F_{001} improves to 70%, which further improves to 80% after sintered at 1230°C. Subsequently, prolonging the soak time is adopted to promote texture development by considering the volatilization of Na and Bi at a higher temperature. A significantly improved texture degree of 90% is achieved at 1230°C with a soak time of 10 h. An increment of the dwelling time to 15 h at 1230°C can further enhance the intensity of (001) and (200) peaks, and at the same time decrease the intensity of all other peaks. This yields a high texture fraction of 95% along ⟨001⟩ direction.

Figure 3 shows the SEM images of the fracture surface for the nontextured and textured NBN ceramics sintered under different conditions. The nontextured ceramic shows good densification characteristics with minor pores and grains of 20–40 μm in size, as given in Fig. 3(a). Smaller grains with size around 5 μm and a large number of pores are observed for the textured ceramic sintered at 1190°C for 5 h, as shown in Fig. 3(b). On this occasion, many plate-like particles with dark contrast (marked with ellipses in orange) are also observed, belonging to NN templates. It should be noticed the NN templates are well aligned and parallel to each other in the matrix, which are beneficial in acquiring a high texture degree during the TGG process. When the sintering temperature increases to 1220°C and 1230°C (Figs. 3(c) and 3(d)), coarser grains with minor pores are observed, accompanied by an abrupt increase in the texture fraction originating from abnormal grain growth.[27] On these occasions, only a few NN templates can be seen, which indicates the NN templates gradually diffuse into the NBN matrix. The NN templates almost vanish by further prolonging the dwelling time to 10 h and 15 h (Figs. 3(e) and 3(f)), indicating the texture degree reaches a saturation in consistence with the high texture degree over 90%.

To investigate the phase transition process, temperature dependence of dielectric permittivity (ε_r) for nontextured and textured ceramics is measured at 10 kHz, as shown in Fig. 4(a). The obvious dielectric peak around 5°C for nontextured ceramic is assigned to be orthorhombic *P* phase to orthorhombic *R* phase transition. This further confirms that the nontextured ceramic is of orthorhombic phase at

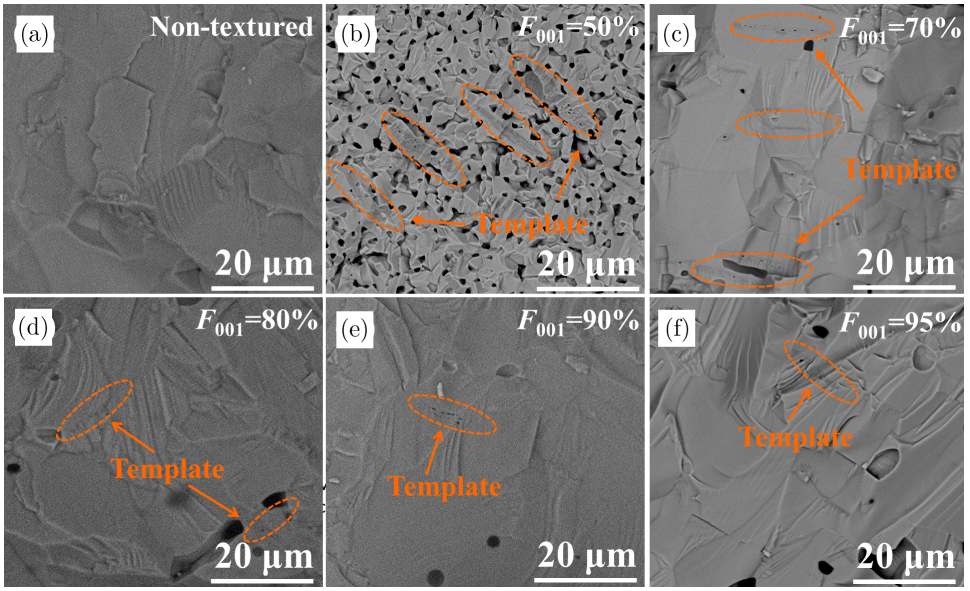

Fig. 3. SEM images of the fracture surface for (a) nontextured NBN ceramics and textured ceramics sintered at different sintered conditions of (b) 1190°C for 5 h, (c) 1220°C for 5 h, (d) 1230°C for 5 h, (e) 1230°C for 10 h and (f) 1230°C for 15 h.

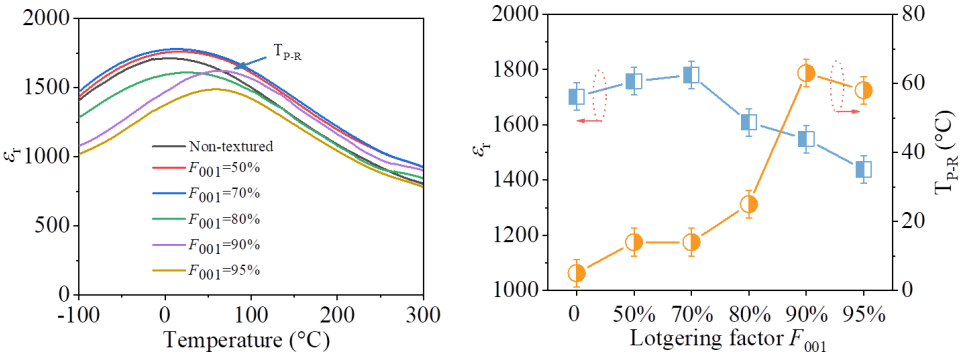

Fig. 4. (a) Dielectric permittivity as a function of temperature for randomly and ⟨001⟩-textured ones with various texture degrees. (b) The T_{P-R} and ε_r as a function of Lotgering factor.

room temperature[32] in consistence with the previous XRD analysis. The textured ceramics exhibit similar temperature dependence of ε_r compared with the nontextured one. In comparison, the textured ceramics show slightly higher phase transition temperature (T_{P-R}). The detailed evolution of T_{P-R} and ε_r at room temperature as a function of the Lotgering factor is shown in Fig. 4(b). The T_{P-R} increases continuously from 14°C for F_{001} = 50% to 58°C for 95% textured ceramics. The evolution of T_{P-R} is associated with the embedding of NN templates into the NBN matrix due to the elevated sintering temperature and prolonged dwelling time, as fewer NN templates are observed in the SEM images. The ε_r increases first and then decreases with the increase of texture degree, reaching a maximum for the 70% textured ceramics.

To evaluate the influence of texture on polarization, the unipolar *P–E* loops are measured at a moderate electric field of 200 kV/cm, as shown in Fig. 5(a). All samples show slim *P–E* loop with small hysteresis. The P_{max} increases from 28.5 μC/cm^2 for the nontextured ceramic to 32.3 μC/cm^2 for 70% textured one, as shown in Fig. 5(b). However, when the Lotgering factor further increases to 80%, the P_{max} decreases to 25.3 μC/cm^2, and a further increase of Lotgering factor to 95% reduces the P_{max} to 22.9 μC/cm^2. The evolution of P_{max} is similar to that of ε_r. The low P_{max} for nontextured ceramic is due to the average polarization.[22] The complex evolution of P_{max} for lower textured ceramics is ascribed to the co-effect of interfacial polarization and clamping effect. According to previous investigations, interfacial polarization is beneficial for boosting polarization, while the clamping effect results in the degradation of polarization.[33,34] In 50% textured ceramic, a large number of interfacial polarization and clamping effect exists due to the addition of NN templates. On this occasion, the interfacial polarization plays a dominant role and leads to a slight increase of P_{max} in comparison to the nontexture one. When the Lotgering factor increases to 70%, the NN templates partly diffuse into the NBN matrix, resulting in a slight decrease of interfacial polarization. On the contrary, the clamping effect also decreases due to the partial dissolution of NN templates and coalescence of grains. Therefore, the balance of the above two factors leads to a further increase in P_{max}. When the Lotgering factor further increases to over 80%, most of the NN templates diffuse into the NBN matrix, which leads to a significant decrease in interfacial polarization and clamping effect. On the other hand, since the ⟨001⟩

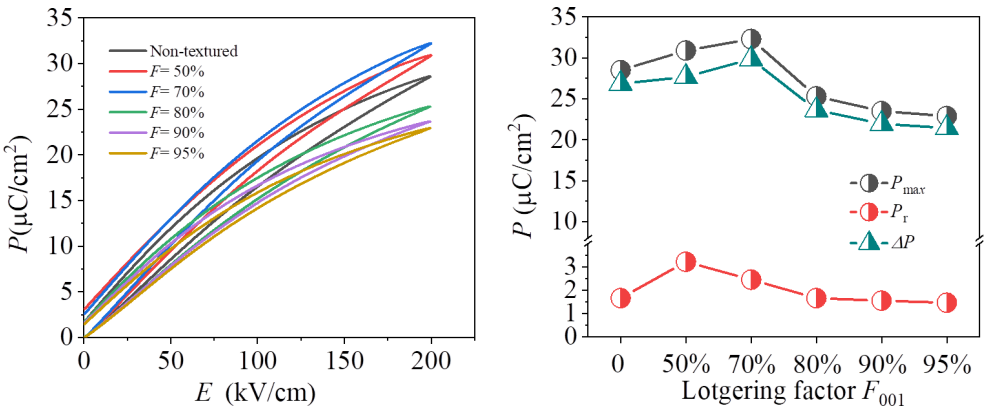

Fig. 5. (a) Unipolar *P–E* hysteresis loops for randomly oriented NBN ceramics and ⟨001⟩-textured ones with various texture degrees at 200 kV/cm. (b) The P_{max}, P_r, and ΔP as a function of texture fraction.

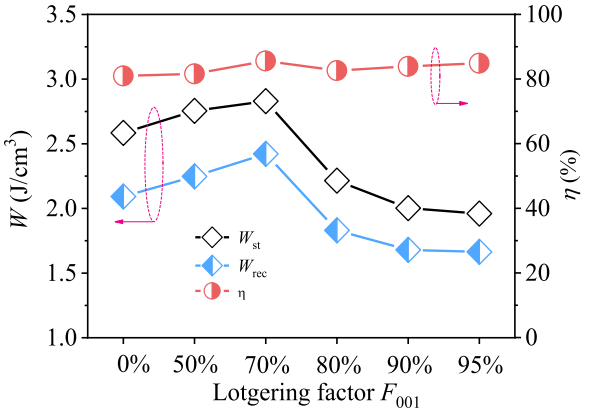

Fig. 6. W, W_{rec} and η for randomly oriented NBN ceramics and ⟨001⟩-textured ones with various texture degrees.

direction is the nonpolar direction for orthorhombic structure, the higher orientation degree ceramics contribute little to the polarization. Therefore, a decrease of P_{max} is observed for 80% textured ceramic and those with higher texture degree. A similar variation of P_r is also observed in the as-prepared ceramics for the same reasons. It's interesting that the gap between P_{max} and P_r ($\Delta P = P_{max} - P_r$) increases first and then decreases with the increase of texture degree.

Figure 6 gives the W_{st}, W_{rec}, and η calculated from the P–E loops. The W_{st} and W_{rec} are 2.6 J/cm^3 and 2.1 J/cm^3 for nontextured ceramic, which respectively increase to 2.8 J/cm^3 and 2.4 J/cm^3 for 70% textured one. After that, both W_{st} and W_{rec} decrease continuously with the increase of texture fraction and finally reduce to 1.9 J/cm^3 and 1.7 J/cm^3 by further improving the texture fraction to 95%. Interestingly, both W_{st} and W_{rec} show a similar variation tendency to P_{max} with the change of texture fraction, indicating that P_{max} is the main factor that affects them. Furthermore, the η shows slight enhancement from 80.9% for random-orientation ceramic to 85.6% for 70% textured one and keeps around 84% for those with higher texture degree.

4. Conclusions

In summary, highly ⟨001⟩-textured NBN ceramics were fabricated by the TGG method. The effect of microstructure and orientation degree on dielectric properties, polarization and energy storage performance was investigated. A relatively low texture degree of 50% was acquired for the textured ceramics sintered at 1190°C for 5 h. When the sintering temperature enhanced to 1230°C and the dwelling time increased to 15 h, the texture degree improved to 95%. The ε_r increased first and then decreased with the increase of texture degree, reaching a maximum for the 70% textured ceramic. The textured ceramic with a Lotgering factor of 70% achieved a high W_{rec} of 2.4 J/cm^3 and η of 85.6%. The excellent energy storage properties of textured ceramic originate from the co-effect of interfacial polarization and clamping effect. This work proves that crystallographic orientation engineering is a potential technique to modify the energy storage properties of dielectric ceramics.

Acknowledgments

This work was financially supported by the National Natural Science Foundation of China (Grant Nos. 52072080 and 11864004) and the Guangxi Natural Science Fund for Distinguished Young Scholars (Grant No. 2022GXNSFFA035034).

Reference

[1]K. Zou, Y. Dan, H. Xu, Q. Zhang, Y. Lu, H. Huang and Y. He, Recent advances in lead-free dielectric materials for energy storage, *Mater. Res. Bull.* **113**, 190 (2019).
[2]Z. Dang, J. Yuan, S. Yao and R. Liao, Flexible nanodielectric materials with high permittivity for power energy storage, *Adv. Mater.* **25**, 6334 (2013).
[3]N. Luo, K. Han, F. Zhuo, C. Xu, G. Zhang, L. J. Liu, X. Chen, C. Hu, H. Zhou and Y. Wei, Aliovalent A-site engineered $AgNbO_3$ lead-free antiferroelectric ceramics toward superior energy storage density, *J. Mater. Chem. A* **7**, 14118 (2019).
[4]Z. Che, L. Ma, G. Luo, C. Xu, Z. Cen, Q. Feng, X. Chen, K. Ren and N. Luo, Phase structure and defect engineering in $(Bi_{0.5}Na_{0.5})$-TiO_3-based relaxor antiferroelectrics toward excellent energy storage performance, *Nano Energy* **100**, 107484 (2022).
[5]P. Zhao, L. Li and X. Wang, $BaTiO_3$–$NaNbO_3$ energy storage ceramics with an ultrafast charge–discharge rate and temperature-stable power density, *Microstruct.* **3**, 2023002 (2022).
[6]S. Zhang, High entropy design: A new pathway to promote the piezoelectricity and dielectric energy storage in perovskite oxides, *Microstruct.* **3**, 2023003 (2022).
[7]Z. Chen, S. Mao, L. Ma, G. Luo, Q. Feng, Z. Cen, F. Toyohisa, X. Peng, L. Liu, H. Zhou, C. Hu and N. Luo, Phase engineering in $NaNbO_3$ antiferroelectrics for high energy storage density, *J. Materiomics* **8**, 753 (2022).
[8]H. Chen, J. Shi, X. Dong, F. Pang, H. Zhang, X. Chen and H. Zhou, Enhanced thermal and frequency stability and decent fatigue endurance in lead-free $NaNbO_3$-based ceramics with high energy storage density and efficiency, *J. Materiomics* **8**, 489 (2022).
[9]H. Qi and R. Z. Zuo, Evolving antiferroelectric stability and phase transition behavior in $NaNbO_3$–$BaZrO_3$–$CaZrO_3$ lead-free ceramics, *J. Eur. Ceram. Soc.* **39**, 2318 (2019).
[10]L. Gao, H. Guo, S. Zhang and C. A. Randall, Stabilized antiferroelectricity in $x BiScO_3$–$(1-x)NaNbO_3$ lead-free ceramics with established double hysteresis loops, *Appl. Phys. Lett.* **112**, 092905 (2018).
[11]J. Ye, G. Wang, X. Chen, F. Cao and X. Dong, Enhanced antiferroelectricity and double hysteresis loop observed in lead-free $(1-x)NaNbO_3$–$xCaSnO_3$ ceramics, *Appl. Phys. Lett.* **114**, 122901 (2019).
[12]H. Qi, R. Z. Zuo, A. W. Xie, A. Tian, J. Fu, Y. Zhang and S. J. Zhang, Ultrahigh energy-storage density in $NaNbO_3$-based lead-free relaxor antiferroelectric ceramics with nanoscale domains, *Adv. Funct. Mater.* **29**, 1903877 (2019).
[13]H. Shimizu, K. Kobayashi, Y. Mizuno, C. A. Randall and G. L. Brennecka, Advantages of low partial pressure of oxygen processing of alkali niobate: $NaNbO_3$, *J. Am. Ceram. Soc.* **97**, 1791 (2014).

[14]T. Hungría, M. Algueró and A. Castro, Grain growth control in $NaNbO_3$–$SrTiO_3$ ceramics by mechanosynthesis and spark plasma sintering, *J. Am. Ceram. Soc.* **90**, 2122 (2007).
[15]W. Liu, Dielectric and sintering properties of $NaNbO_3$ ceramic prepared by Pechini method, *J. Electroceram.* **31**, 376 (2013).
[16]X. Tang, N. Luo, Q. Feng, X. Chen and Y. Wei, Microstructure and electrical property of $NaNbO_3$ ceramics prepared by cold sintering process assisted post-heat-treatment, *J. Alloys Compd.* **877**, 160284 (2021).
[17]A. Xie, H. Qi and R. Zuo, Achieving remarkable amplification of energy-storage density in two-step sintered $NaNbO_3$–$SrTiO_3$ antiferroelectric capacitors through dual adjustment of local heterogeneity and grain scale, *ACS Appl. Mater. Interfaces* **12**, 19467 (2020).
[18]Y. Sun, Y. Chang, J. Wu, Y. Liu, L. Jin, S. Zhang, B. Yang and W. Cao, Ultrahigh energy harvesting properties in textured lead-free piezoelectric composites, *J. Mater. Chem. A* **7**, 3603 (2019).
[19]F. Guan, J. Pan, J. Wang, Q. Wang and L. Zhu, Crystal orientation effect on electric energy storage in poly(vinylidene fluoride-co-hexafluoropropylene) copolymers, *Macromolecules* **43**, 384 (2009).
[20]P. Li, J. Zhai, B. Shen, S. Zhang, X. Li, F. Zhu and X. Zhang, Ultrahigh piezoelectric properties in textured (K,Na)NbO_3-based lead-free ceramics, *Adv. Mater.* **30**, 1705171 (2018).
[21]Y. Liu, Y. Chang, E. Sun, F. Li, S. Zhang, B. Yang, Y. Sun, J. Wu and W. Cao, Significantly enhanced energy-harvesting performance and superior fatigue-resistant behavior in $[001]_c$-textured $BaTiO_3$-based lead-free piezoceramics, *ACS Appl. Mater. Interfaces* **10**, 31488 (2018).
[22]Y. Yan, J. Zhou, D. Maurya, Y. Wang and S. Priya, Giant piezoelectric voltage coefficient in grain-oriented modified $PbTiO_3$ material, *Nat. Commun.* **7**, 13089 (2016).
[23]P. Li, B. Liu, B. Shen, J. Zhai, Y. Zhang, F. Li and X. Liu, Mechanism of significantly enhanced piezoelectric performance and stability in textured potassium–sodium niobate piezoelectric ceramics, *J. Eur. Ceram. Soc.* **38**, 75 (2018).
[24]Y. Chang, J. Wu, Y. Sun, S. Zhang, X. Wang, B. Yang, G. Messing and W. Cao, Enhanced electromechanical properties and phase transition temperatures in [001] textured $Pb(In_{1/2}Nb_{1/2})O_3$–$Pb(Mg_{1/3}Nb_{2/3})O_3$–$PbTiO_3$ ternary ceramics, *Appl. Phys. Lett.* **107**, 082902 (2015).
[25]J. Li, Z. Shen, X. Chen, S. Yang, W. Zhou, M. Wang, L. Wang, Q. Kou, Y. Liu, Q. Li, Z. Xu, Y. Chang, S. Zhang and F. Li, Grain-orientation-engineered multilayer ceramic capacitors for energy storage applications, *Nat. Mater.* **19**, 999 (2020).
[26]W. Bai, D. Chen, P. Li, B. Shen, J. Zhai and Z. Ji, Enhanced electromechanical properties in ⟨00l⟩-textured $(Ba_{0.85}Ca_{0.15})(Zr_{0.1}Ti_{0.9})O_3$ lead-free piezoceramics, *Ceram. Int.* **42**, 3429 (2016).
[27]T. Kimura, Y. Sakuma, H. Muramatsu and Y. Miura, Mechanisms of texture development in ceramics prepared by templated grain growth method, *Key Eng. Mater.* **269**, 177 (2004).
[28]Y. Chang, Z. Yang, X. Chao, Z. Liu and Z. Wang, Synthesis and morphology of anisotropic $NaNbO_3$ seed crystals, *Mater. Chem. Phys.* **111**, 195 (2008).
[29]N. Wei, T. Karaki and T. Fujii, Fabrication of textured (K,Na)NbO_3-based ceramics at low sintering temperatures by using $NaNbO_3$ templates prepared with hydrothermal method, *Jpn. J. Appl. Phys.* **61**, SN1018 (2022).
[30]H. Leng, Y. Yan, M. Fanton and S. Priya, Polarization fatigue mechanism of high-power textured piezoelectric ceramics, *ACS Appl. Electron. Mater.* **4**, 1047 (2022).
[31]F. Lotgering, Topotactical reactions with ferrimagnetic oxides having hexagonal crystal structures — I, *J. Inorg. Nucl. Chem.* **9**, 113 (1959).
[32]H. Qi, A. Xie, J. Fu and R. Zuo, Emerging antiferroelectric phases with fascinating dielectric, polarization and strain response in $NaNbO_3$–$(Bi_{0.5}Na_{0.5})TiO_3$ lead-free binary system, *Acta Mater.* **208**, 116710 (2021).
[33]Z. Wang, M. Kong, X. Wang, Y. Li, Z. Yi and Z. Sun, Ultrahigh energy storage performance in gradient textured composites of plate-like $Na_{0.5}Bi_{4.5}Ti_4O_{15}$/PVDF through interface engineering, *Ceram. Int.* **47**, 8787 (2021).
[34]Y. Yan, Y. Zhou, S. Gupta and S. Priya, Fatigue mechanism of textured $Pb(Mg_{1/3}Nb_{2/3})O_3$–$PbTiO_3$ ceramics, *Appl. Phys. Lett.* **103**, 082906 (2013).